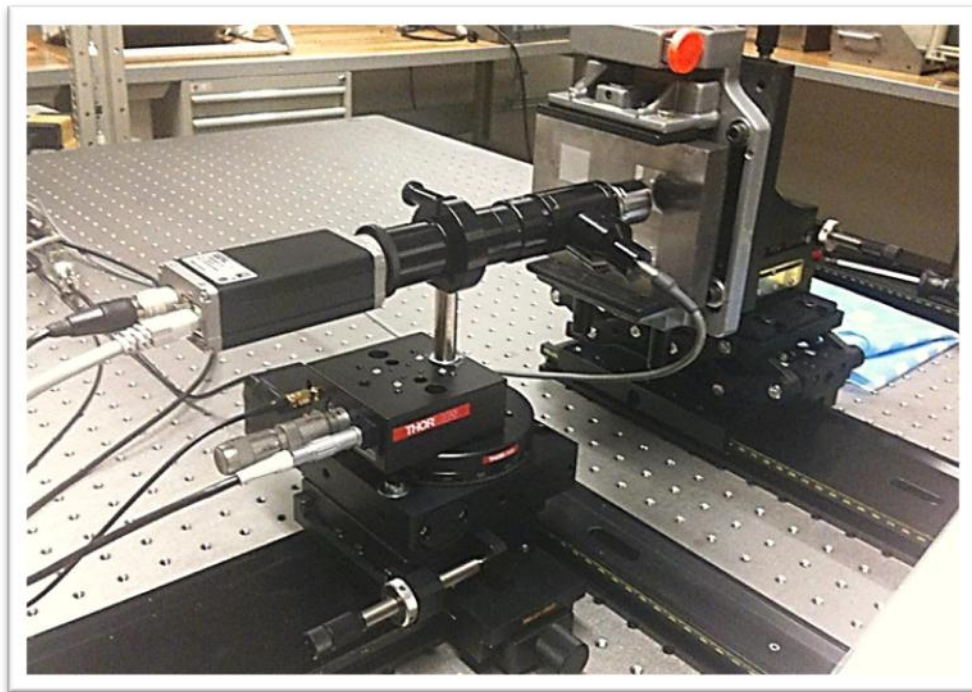

Technical report, IDE1065, November 2010

Construction and Validation of a White Light Interferometer

Master's Thesis in Electrical Engineering

Karthick Sathiamoorthy & Tanjim Ahmed

Supervisor: Lars Bååth



School of Information Science, Computer and Electrical Engineering
Halmstad University

Construction and Validation of a White Light Interferometer

Master's thesis in Electrical Engineering

School of Information Science, Computer and Electrical Engineering
Halmstad University
Box 823, S-301 18 Halmstad, Sweden

December 2010

Description of cover page picture: Image of Prototype White Light Interferometer

Preface

The developments in photonics have helped mankind to break engineering barriers in the field of electronics and communication which were not realized with electronics alone. The advances in science aim at achieving greater speed of operation and reduced form factor for systems in various fields. These achievements were feasible only by the developments of diagnostic instruments which can analyze physical structure down to nanometers. Photonics plays a major role in this sector since it uses the wavelength of light as its reference for measurements. Pursuing the master program in Microelectronics and Photonics at Halmstad University, we were most interested in Optics and Photonics. Working on the interferometers was very interesting and we hope this project will be useful for future work and research in this area of science.

Karthick Sathiamoorthy

Tanjim Ahmed

Halmstad University, December 2010

Acknowledgements

First and foremost, we would like to express our extreme gratitude towards our research supervisor prof. Lars Bååth, who has been a very encouraging and motivating advisor. His ideas for excellence and perfection are highly valuable and have helped us bring the project to this level of completion. His availability for us at all time has helped us finish this project more swiftly.

We would also like to thank Sameera Atrajji, who was always around to point us to helpful resources and experts in different fields. We are thankful to Stefan Rosén for his introduction on ADE Phaseshift's interferometric topographer, MicroXAM. We are also thankful to Sabina Rebeggiani for her help with the use of MountainsMap software. Finally we would like to thank our thesis coordinator, prof. Håkan Petersson and dr. Lars Landin for their valuable suggestion on the samples needed for validation.

Abstract

White light interferometry is a well-developed and very old technique for optical measurements. The thesis describes the design of a vertical scan interferometer system to study the surface topography of surfaces down to nanometers. The desired properties of the system are its simplicity, portability and compact size, making it suitable for use in general labs and for educational purposes. By acquiring a sequence of images of the deformed fringe pattern, the surface topography can be observed, giving greater understanding of the surface roughness.

The principle behind the system is coherence peak sensing where the resulting fringe pattern of the object gets changed in accordance with its surface topography. To accomplish this, individual components of the interferometer were studied and a prototype was built in the lab. A series of experiments were performed which validate the working of the system. The results of the validation which are produced in the report give the accuracy of the system. The output from the prototype interferometer is processed by MATLAB to decode the surface topography of the object under measurement. The design of the prototype is also discussed. Possible application of this device for sensing the surface topography of a cylindrical object is also put forward.

Even-though the white light interferometer is more common, making them simple and cost effective will be more advantageous for the whole research community.

Abbreviations

CCD – Charge Coupled **D**evice

OPD – Optical **P**ath **D**ifference

PZT – Piezoelectric **T**ransducer

LED – Light **E**mitting **D**iode

GUI – Graphical **U**ser **I**nterface

AVI – Audio **V**ideo **I**nterleave (file format)

Content

1 Introduction	1
1.1 Goals	1
2 Light Interferometry System	1
2.1 Superposition of waves	1
2.2 Coherence	3
2.2.1 Temporal coherence.....	3
2.2.2 Spatial coherence	4
2.3 Theory of Optical Interference.....	6
3 White Light Interferometry	10
3.1 Advantages of using a white light source	13
3.2 Interference Objectives	14
3.3 White-Light Interferometry Equation.....	16
3.4 MicroXAM interferometer from ADE Phase Shift	18
3.5 Prototype Coherence Peak Scanning Interferometer	18
3.5.1 Setup	18
3.5.2 Interferometer Objective	20
3.5.3 Camera	20
3.5.4 Rotor table controller	20
3.5.5 Piezo drive system	20
4 Measurements	20
4.1 Object under measurement	20
4.2 Programming the Scanning System	21
4.3 Post processing.....	24
4.4 Results from Prototype Interferometer	26
4.5 Validation of the prototype interferometer	27
4.5.1 Transformation of matrix.....	29
4.5.2 Observations	32
5 Possible Design	33
6 Conclusion	35
7 Reference	36

List of Figures

Figure 1	Path of light in Michelson interferometer [16].....	2
Figure 2	Example for constructive and destructive interference [16].....	2
Figure 3	Image of a general interferogram [16].....	3
Figure 4	Temporal coherence of two waves with coherence time τ_c [16]	4
Figure 5a	A laser beam with spatial and temporal coherence [15].....	5
Figure 5b	A laser beam with spatial coherence, but poor temporal coherence [15].....	5
Figure 5c	A laser beam with poor spatial coherence, but good temporal coherence [15]	5
Figure 6	Young's Double Slit Experiment	7
Figure 7	Basic Principle of Michelson and Twyman Interferometers	8
Figure 8	Michelson interferometer with an extended source.....	9
Figure 9	The Twyman-Green interferometer, as used to test a prism	10
Figure 10	Schematic diagram of an interference microscope [16]	11
Figure 11	The amplitude of interferogram with respect to the optical path distance [17].....	12
Figure 12a	The Michelson objective [12].....	14
Figure 12b	The Mirau objective [12].....	15
Figure 12c	The Linnik objective [12]	15
Figure 13	A raw image of the surface with the intensity envelope	17
Figure 14	The prototype interferometer setup	19
Figure 15	The sample and the reference mirror setup in a Mirau objective [16]	19
Figure 16	Sample surface taken as a test object	21
Figure 17a	User interface on LabView for piezo stage control	21
Figure 17b	The control schematic in LabView for piezo stage control.....	23
Figure 18	Construction of 3-D surface through fringe modulation intensity scanning [18].....	24
Figure 19	The processing of interferogram for 3D surface construction.....	25
Figure 20a	The constructed 3D surface of the examined object.....	26
Figure 20b	The constructed 3D surface from MicroXAM data	27
Figure 21	The process of comparison of results of the two interferogram.....	28
Figure 22	The process matrix transformation by pairing of points	29
Figure 23	The transformed image of the matrix	30
Figure 24	The difference between the two results as a grayscale image	31
Figure 25	The dust spots on the beam splitter	33
Figure 26	The possible design of the interferometer to scan a cylindrical surface.....	34

1 Introduction

White light interferometry is a widely used technique for measurement of surface topography of objects over large areas. Systems which use this technique can measure areas which are equal to the field of view of the instrument. Interferometric optical topographers are widely used to study surface topography due to the high measurement accuracy, non-contact, rapid data acquisition and analysis.

Even though the conventional interferometers are extensively used they are built for ruggedness and have many features and different techniques of measurement integrated which are not effectively used by all. Moreover they have features for automated adjustment which can be done manually to some extent.

In this project we try to replicate the white light interferometer by constructing a prototype in the lab based on the white interferometry measurement technique. With measurement results from the constructed interferometer the feasibility for practical usage is discussed.

The report also presents the use of the technology on surfaces and analyzes the accuracy of the prototype compared with the commercial interferometer (MicroXAM).

1.1 Goals

Aim of this project is to construct a coherence peak white light interferometer and define its accuracy. To achieve this goal this project includes the design, construction, experiments and validation of the interferometer system.

2 Light Interferometry System

Interferometry is the technique of analyzing the properties of two or more waves by studying the pattern of interference resulting from their superposition. The instrument that uses this concept is known as an interferometer.

2.1 Superposition of waves

The principle of superposition combines separate waves so that the result of their combination has meaningful information about the original state of the waves. The resulting interference pattern represents the difference in phase between the two waves of same frequency. The waves which are in phase will result in constructive interference

while waves which are out of phase will result in a destructive interference. Common interferometers use light as diagnostic element to examine the surface topography [1].

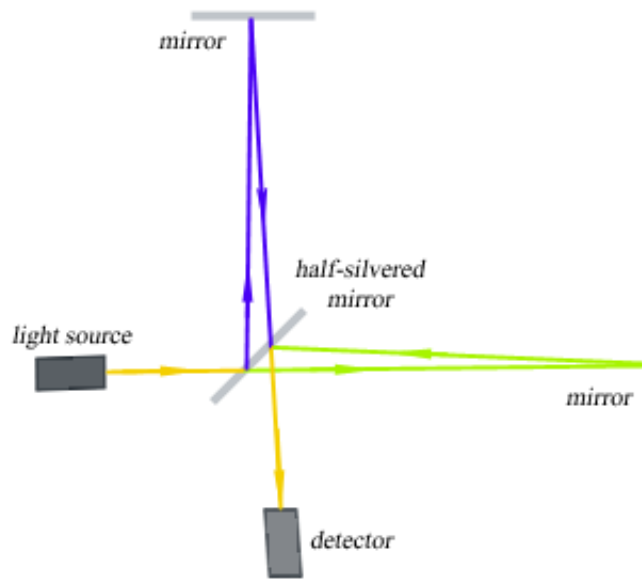


Figure 1 - Path of light in Michelson interferometer [16]

Normally a single beam of coherent light will be divided into two identical beams by a partial mirror or a grating as shown in figure 1. Each of these beams will travel a different path, until they are recombined before arriving at the detector. The optical path difference between the beams creates a corresponding phase difference between them. It is this phase difference between the initially identical waves that creates the interference. The interference of waves with zero phase difference and waves which are completely out of phase is shown in figure 2.

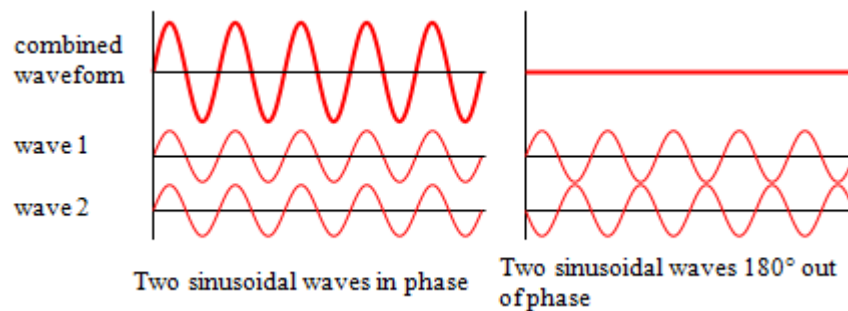


Figure 2 – Example for constructive and destructive interference [16]

If a single beam has been divided into two then the phase difference is diagnostic of the changes in phase along the paths. This can be a change in the path length itself or a change in the refractive index along the path. The resulting interferogram might look like the one in figure 3.

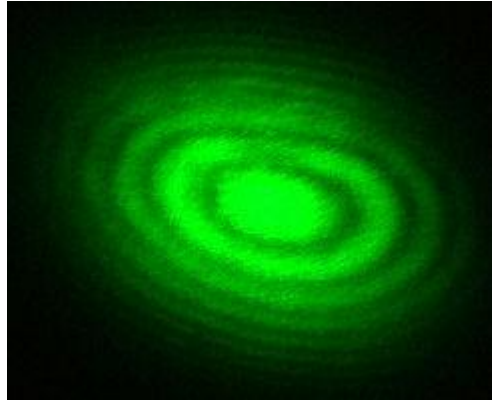


Figure 3 – Image of a general interferogram [16]

2.2 Coherence

To obtain a fringe pattern the two sources need to be in phase or should have a constant relative phase between them. This property of waves always marching together is called coherence and it is a fundamental requirement for the sources producing interference. The coherence of the interfering beams determines the fringe contrast and sharpness. Common sources produce light that is a mix of photon wavetrains exhibiting different frequency.

A fixed phase relationship between the waves at different locations or at different times defines coherence.

2.2.1 Temporal coherence

At each point of the light in space there is a net field that oscillates nicely resembling a sinusoidal wave before it randomly changes phase and this measure is known as temporal coherence. The average time interval during which the light wave oscillates in a predictable way we have already designated as the coherence time of the radiation (τ_c). The longer the coherence time, the greater the temporal coherence of the source. The corresponding spatial extent over which the lightwave oscillates in a regular, predictable way is the coherence length.

$$\tau_c \Delta f \approx 1$$

The above equation shows that the faster a wave decorrelates (and hence the smaller τ_c is) the larger the range of frequencies Δf the wave contains. The figure below shows two waves of slightly different frequencies having a temporal coherence time τ_c .

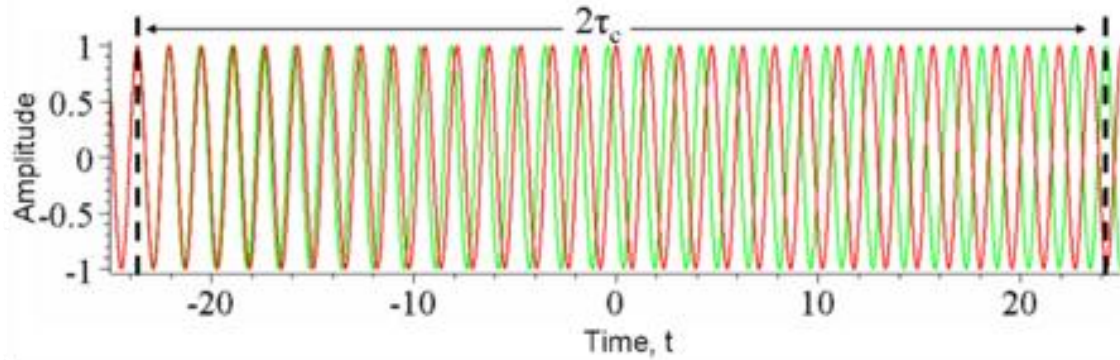


Figure 4 – Temporal coherence of two waves with coherence time τ_c [16]

Simply, the temporal coherence is a manifestation of the spectral purity of the light source. In contrast, if the light was ideally monochromatic, the wave would be a perfect sinusoid with an infinite coherence length [2].

Temporal coherence is a strong correlation between the disturbances at one location but at different times. In white light interferometry the temporal coherence of the white light defines the extent to which the fringes are visible in the field of view of the focused surface.

2.2.2 Spatial coherence

For point sources of light the disturbances at the points on its wavefront is completely correlated and so these laterally separated points are in-phase and stay in-phase. So if we consider a point source which changes the frequency moment to moment, even then the waves exhibit complete spatial coherence.

By contrast, suppose the source is broad, that is, composed of many widely spaced point sources, the disturbance at laterally spaced point will be completely uncorrelated depending on the size of the source.

Spatial coherence therefore means a strong correlation in phase between the waves at different locations across the beam profile.

Given below are examples to better understand the types of coherence.

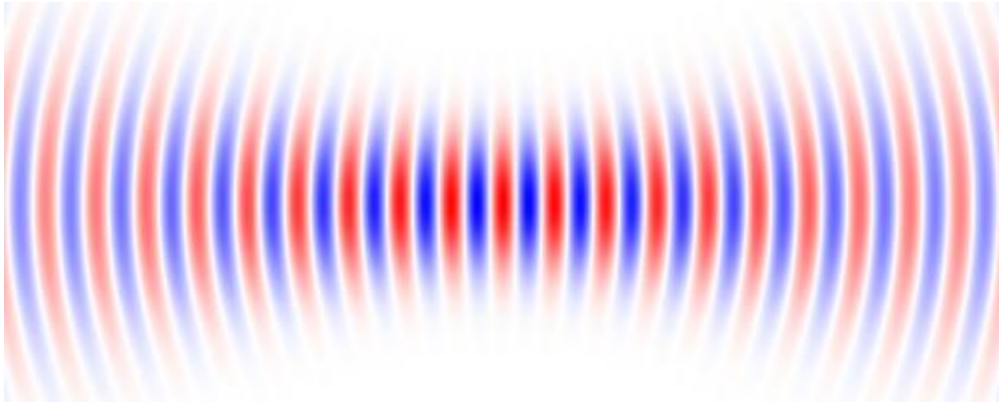


Figure 5a - A laser beam with spatial and temporal coherence [15]

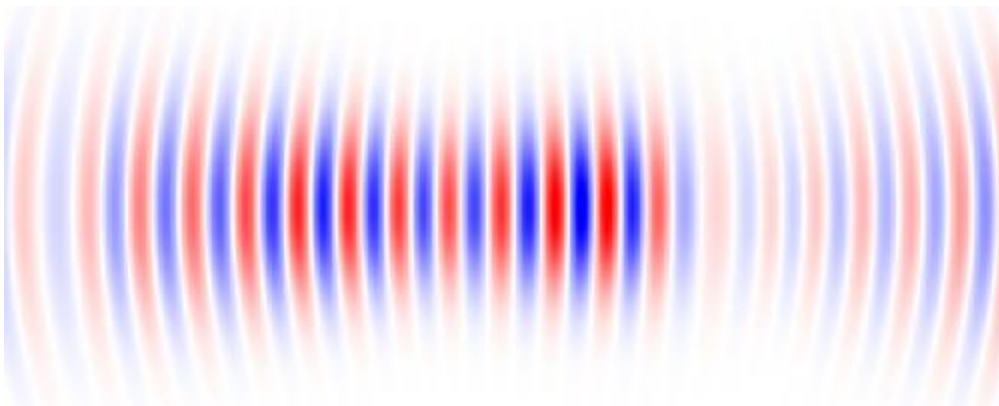


Figure 5b - A laser beam with spatial coherence, but poor temporal coherence [15]

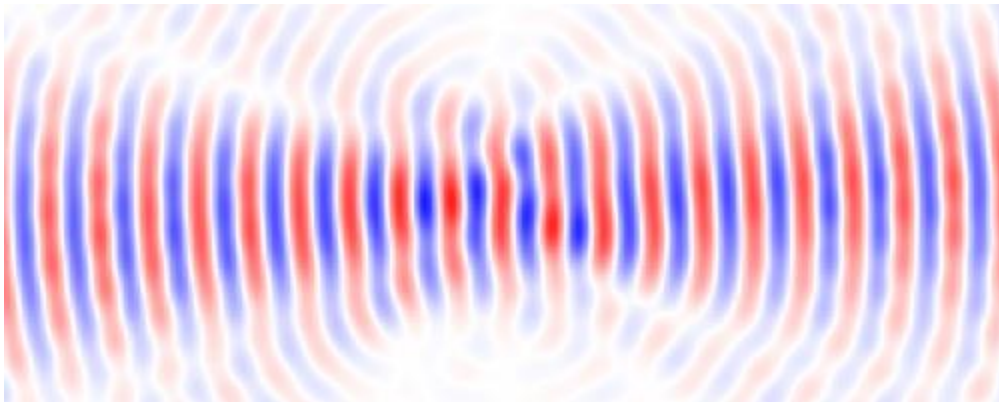


Figure 5c - A laser beam with poor spatial coherence, but good temporal coherence [15]

2.3 Theory of Optical Interference

When light from a source is split into two beams, then the inherent variation in the two beams are generally correlated, and the beams are said to be completely or partially coherent depending on the existing correlation. In light beams from two independent sources, the phase functions are usually uncorrelated and such beams are called incoherent beams. When coherent waves superpose, they produce visible interference effects because their amplitudes can combine, whereas for the incoherent waves, their intensities combine. Interference produced by incoherent waves varies too rapidly in time to be practically observed.

When two mutually coherent beams pass through a point, we can observe the phenomena of interference between the wavefront. The medium at that point is subjected to the total effect of the superposition of the two vibrations, and under certain conditions, this superposition results in stationary waves, known as interference fringes.

Consider the superposition of two monochromatic plane waves U_1 and U_2 of the same frequency and with different complex amplitudes. The result is a monochromatic wave of the same frequency and the complex amplitude is the sum of the individual amplitudes, i.e.

$$U(\vec{r}) = U_1(\vec{r}) + U_2(\vec{r})$$

Expressing the plane waves in terms of their intensities, we get

$$I_1 = \langle U_1 U_1^* \rangle_T$$

$$I_2 = \langle U_2 U_2^* \rangle_T$$

Thus we have,

$$I = |U|^2 = \langle (U_1 + U_2)(U_1 + U_2)^* \rangle_T$$

where the asterisk denotes complex conjugation.

If,

$$U_1 = \sqrt{I_1} e^{j\phi_1}$$

$$U_2 = \sqrt{I_2} e^{j\phi_2}$$

Then

$$I = I_1 + I_2 + 2\sqrt{I_1 I_2} \cos \phi$$

where

$$\phi = \phi_1 - \phi_2$$

The above equation is known as the interference equation, and the term

$$2\sqrt{I_1 I_2} \cos \phi$$

is known as the interference term. At different points in space, the resultant irradiance can be greater, less than or equal to $I_1 + I_2$, depending on the value of the interference term, i.e. depending on ϕ . Irradiance maxima occur for $\phi = 2\pi m$ and minima occur for $\phi = (2m+1)\pi$. The dark and light zones that would be seen on a screen placed in the region of interference are known as interference fringes.

An interferometer is, in the broadest sense, a device that generates interference fringes. Interferometers can basically be classified into two types: wavefront splitting interferometers and amplitude splitting interferometers.

Wavefront splitting interferometers recombine two different parts of a wavefront to produce fringes. The earliest experimental arrangement for demonstrating the interference of light was Young's experiment, which employed a double slit to obtain two sources of light. The principle of double slit experiment is illustrated in figure 6.

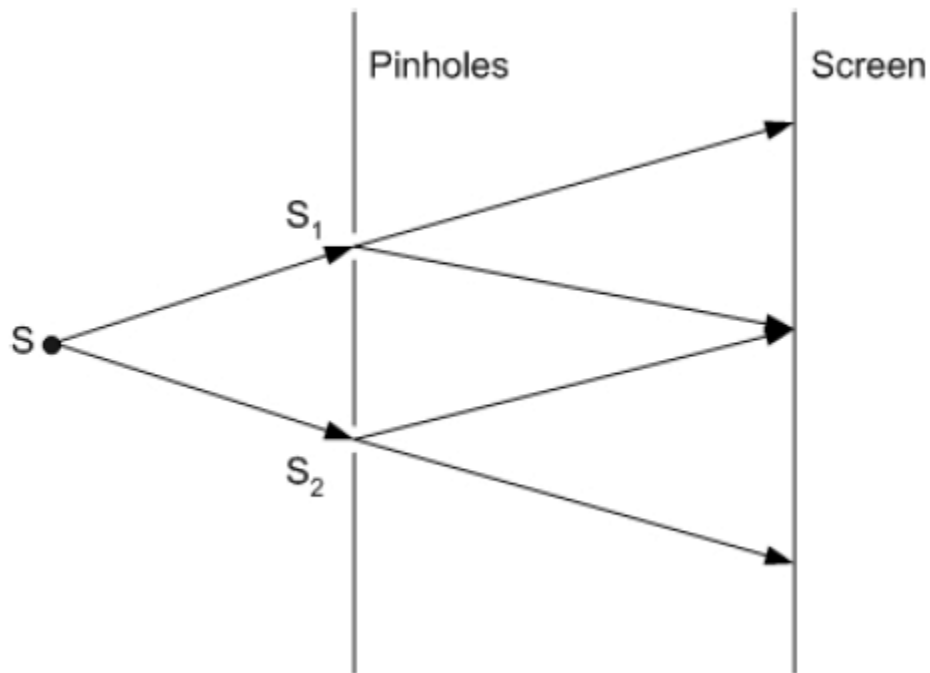


Figure 6 - Young's Double Slit Experiment

The light from a monochromatic source S falls on the two pinholes S_1 and S_2 , which are close together and equidistant from S . The pinholes act as secondary monochromatic sources, which are in phase when $SS_1=SS_2$, and the beams from these sources are superposed in the region beyond the pinholes. An interference pattern can be observed on the screen.

Amplitude-splitting interferometers, on the other hand, divide a wavefront into two beams (splitting the amplitude), which propagate through separate paths and are then recombined. Typically, beam splitters are used for splitting and recombining wavefront amplitudes.

One of the most important interferometers based on amplitude-splitting technique is the Michelson's interferometer. Its basic arrangement is shown in figure 7.

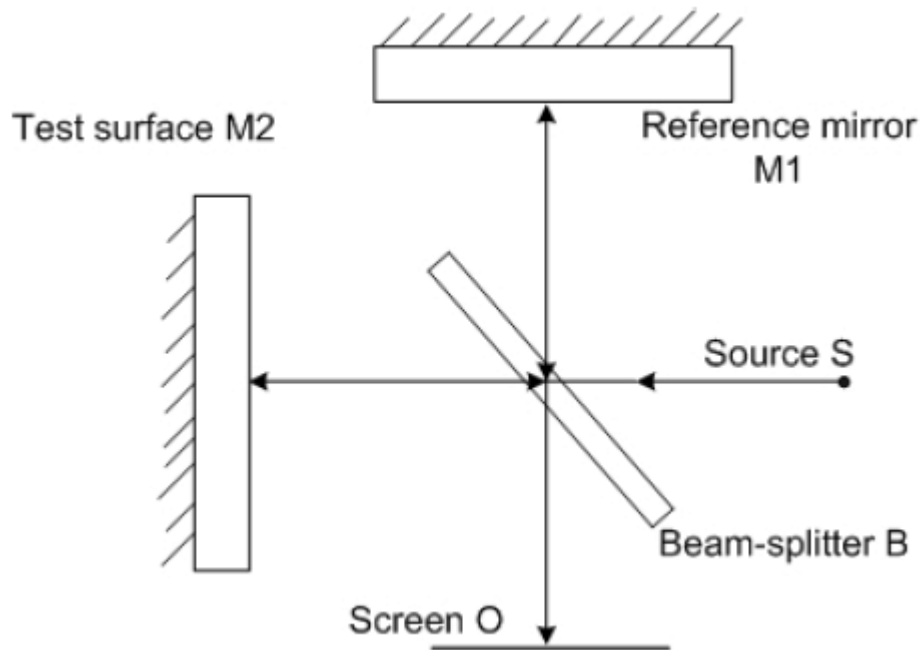


Figure 7 - Basic Principle of Michelson and Twyman Interferometers

It consists of a partially silvered mirror B , which acts as a beam splitter, dividing the incident beam coming from S into two beams of equal intensity, one reflected and the other transmitted. These beams strike the reference mirror $M1$ and the test surface $M2$ at normal incidence and are reflected back and meet at the beam splitter and combine to create interference patterns, which can be seen at the point of observation O .

In figure 7, the interferometer is set up with a point source, which would illuminate only a small part of the field of view. Hence this configuration is used only after further modification. If an extended source (a source with uniform surface brightness) is used in

Michelson's mirror arrangement, the form is as shown in figure 8. In this arrangement utilizing an extended source, the rays, which reach the point of observation, leave the mirrors at various angles.

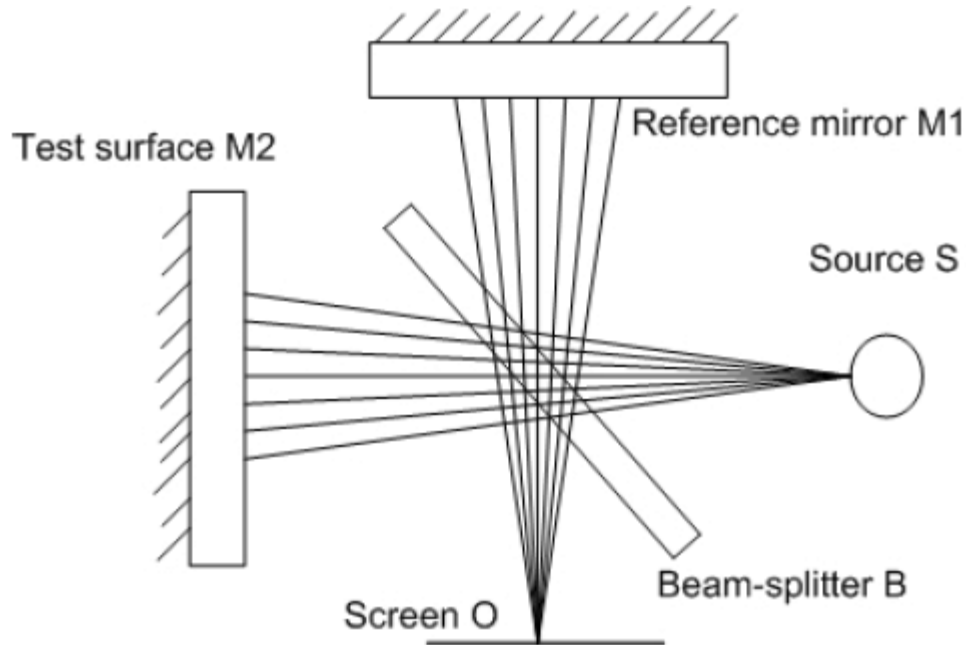


Figure 8 - Michelson interferometer with an extended source

A Michelson's interferometer modified to work in collimated light is a Twyman-Green interferometer. In the Twyman-Green interferometer, a point source is placed at the focus of a lens so that a plane wave front traverses the mirror system. On reaching the second lens, the wave front is again made spherical and converges on the observation screen. The Twyman-Green interferometer is shown below. In its simplest form, it can be used to test plane mirrors, plane-parallel windows, or prisms. The figure 9 illustrates its use in testing of a prism.

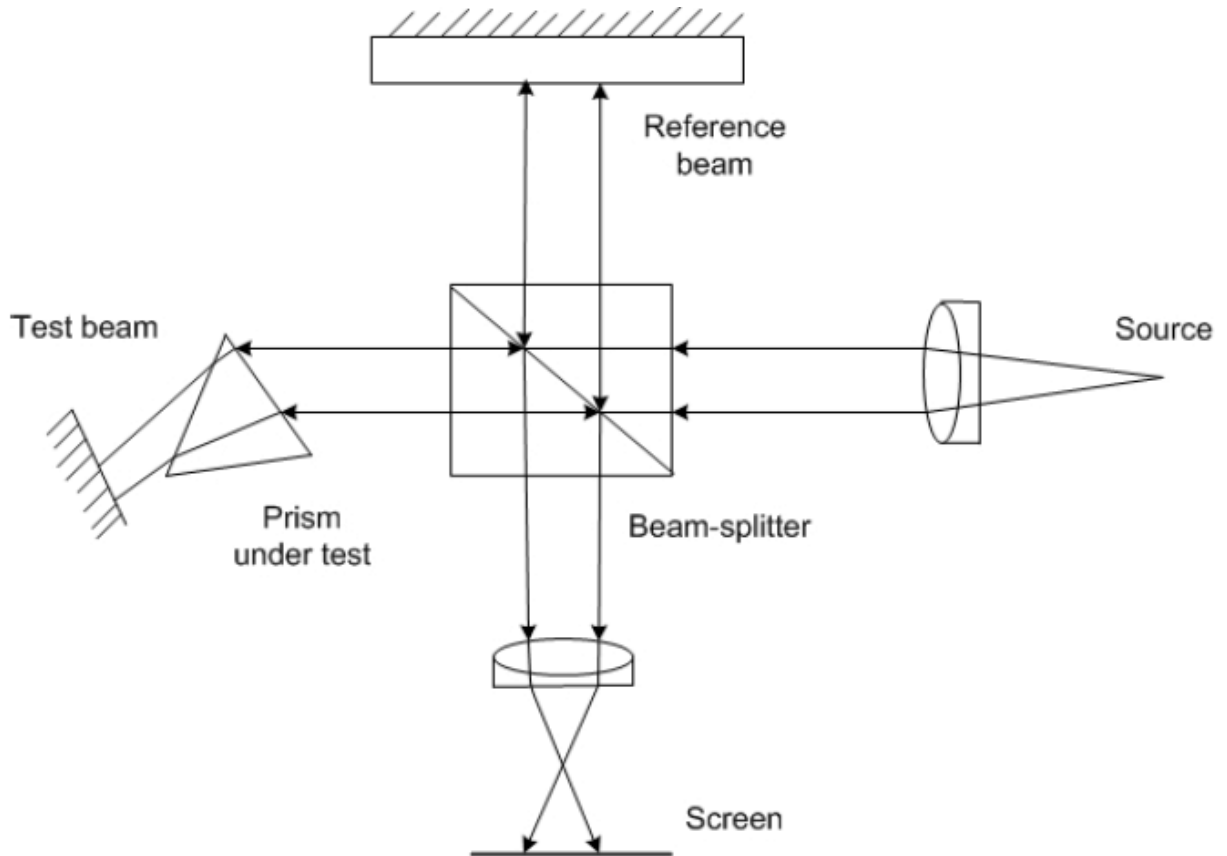


Figure 9 - The Twyman-Green interferometer, as used to test a prism

3 White Light Interferometry

For an interferometer to be a true white light achromatic interferometer two conditions need to be satisfied.

First, the position of the zero order interference fringes must be independent of wavelength. Second, the spacing of the interference fringes must be independent of wavelength. That is, the position of all interference fringes, independent of order number, is independent of wavelength. Generally, in a white light interferometer only the first condition is satisfied and we do not have a truly achromatic interferometer.

The basic technique involves splitting an optical beam from the same source into two separate beams – one of the beams is passed through, or reflected from, the object to be measured whilst the other beam (the reference) follows a known and constant optical path. The same basic principle can be used in a microscope arrangement as shown in figure 10.

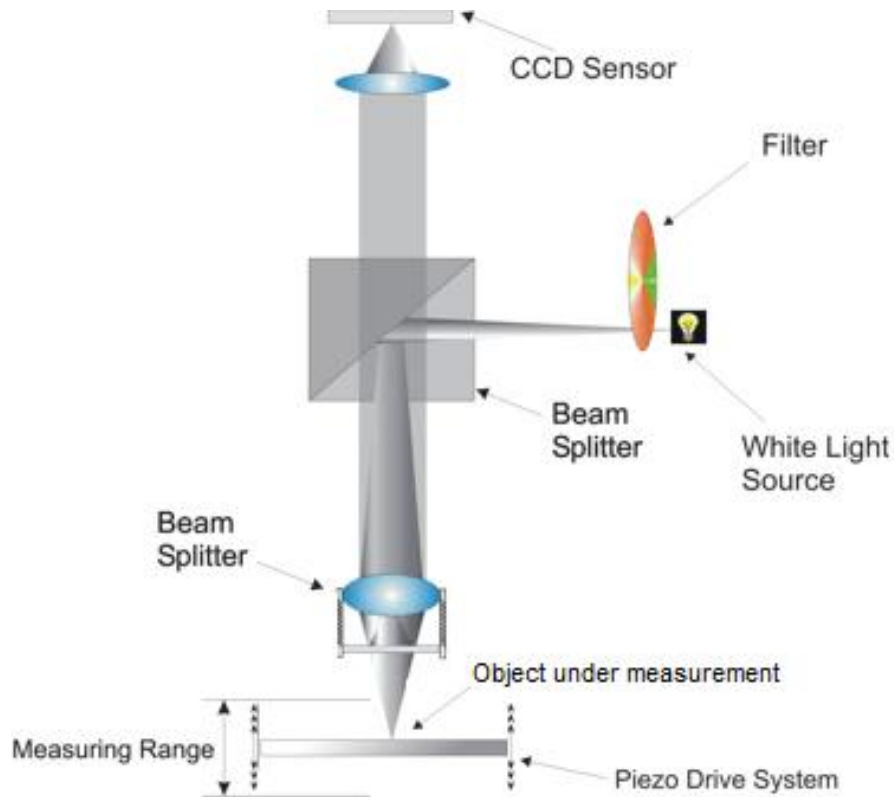


Figure 10 - Schematic diagram of an interference microscope [16]

Here a light source provides a beam which is passed through a filter and reflected by the upper beam splitter (acting essentially as a mirror at this stage) down to the objective lens. The lower beam splitter in the objective lens creates and combines the light beams reflected from the sample surface and the reference.

This creates an interference pattern called an interferogram which is magnified by the microscope optics and finally imaged by the CCD camera. This static fringe image would show differences in distance apart of the reference and sample – essentially revealing local ‘bow and warp’ of the sample. However if the objective lens is moved vertically the path length between sample and beam splitter changes and creates a series of moving interference fringes which will be detected by the camera. The aim is to establish the point at which maximum constructive interference occurs (i.e. at which the image is brightest). The figure 11 gives the irradiance at a single sample point as the sample is translated through focus varying the Optical Path Distance (OPD).

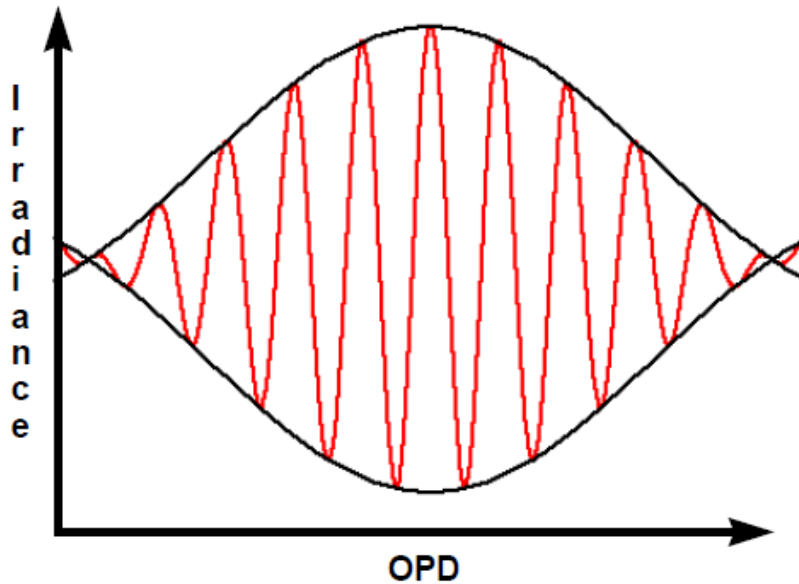


Figure 11 – The amplitude of interferogram with respect to the optical path distance [17]

Once this is achieved, provided the vertical movement of the lens can be accurately tracked, it is possible to create a 3D map of the sample surface by measuring the position of the lens required to produce the brightest image at each point on the CCD array. This would normally be carried out using a monochromatic light source – however there could be several different positions at which a maximum in the signal would occur. By using multiple wavelengths (and white light is the ultimate case) it is possible to set the system up so that there is only one point at which this maximum occurs. The only limit on the achievable height resolution is set by how well the measurement algorithm can define the maximum brightness (and thus the surface position) as the objective lens is scanned vertically using a piezo-electric drive. Each pixel of the CCD array effectively acts as an individual interferometer and thus builds up a very accurate map of the surface [3] [4] [5] [6] [7].

The processing of the interferogram using modern computerized technique has helped to increase the accuracy and the dynamic range of surface topography measurements. In white light interferometry the point of highest fringe contrast, the coherence peak, is the most distinctive feature of the broadband interferogram. Most optical topographers based on white light process the interference data in order to determine the position of the coherence peak [8]. These topographers differ mostly in the way they detect and process the fringe-contrast envelope. Balasubramanian makes the reference mirror oscillate with a PZT to calculate the fringe contrast, and then repeats the calculation for a succession of points in space in order to trace out the contrast envelope [9]. Caber has developed more flexible and accurate formulas for calculating the fringe contrast, and also with more powerful methods of estimating the fringe contrast peak with sparse data using curve fitting [10]. Kino and Chim transform their data to the spatial-frequency domain, eliminate the negative frequencies, center the positive frequency packet on zero and then

transform back to the original data domain to reveal a carrier-suppressed envelope for further processing [11].

3.1 Advantages of using a white light source

Lasers are generally used as the light source for the interferometer system because it is easy to obtain interference fringes due to their long coherence length regardless of the path difference between the two interfering beams. However, there are several advantages of using the white light as the source in interferometric optical topographers.

The first advantage is that the noise due to spurious interference fringes is avoided because the coherence length of white light is very short and interference can be obtained only when the path length are within a few microns or less. [12]. Thus, even though the spurious reflections still exist in the white light interferometer they don't produce fringes which can add to the noise.

For an optical topographer, it is very important that the sample is in focus or else the measurements will be incorrect. It is very difficult to determine the focus on a smooth surface due to the absence of structures. A major advantage here when using white light source is the presence of interference fringes which precisely defines focus. The maximum contrast fringes are obtained only when the path lengths are exactly matched. Hence moving through the sample looking for maximum contrast fringes the correct focus can be obtained. [13].

The third advantage of using a white light is that it can be filtered to produce different wavelengths for measurement on the same sample. Here, the multiple wavelength techniques can be used to measure steps or surfaces having steep slopes [14]. The surface height change allowed in the measurement using a single wavelength is limited to one-quarter wavelength. By performing the measurement at two wavelengths, λ_1 and λ_2 and subtracting the two measurements, the limitation in the height between two adjacent detector points is now one-quarter of λ_{eq} , where

$$\lambda_{eq} = \frac{\lambda_1 \lambda_2}{|\lambda_1 - \lambda_2|}$$

The measurement is essentially tested at a synthesized equivalent wavelength, λ_{eq} . While this technique increases the dynamic range of measurement, it decreases the precision by the ratio of λ_{eq}/λ . The precision can be regained by using the equivalent wavelength results to correct the 2π ambiguities of the single wavelength data. Thus a large dynamic range is obtained maintaining the precision of single wavelength data. [12]

3.2 Interference Objectives

An important component in an interferometer optical topographer is the microscope interference objective. Due to wide range of optical topographic measurements, no single type of interferometer objective can be used.

The Michelson interferometer is used for low magnifications such as 1.5X, 2.5X and 5X. Advantage of this interferometer is that only a single objective is used and hence first order aberrations do not contribute to errors in measurements. Only long working distance objectives can be used because the beam splitter must be placed between the objective and sample.

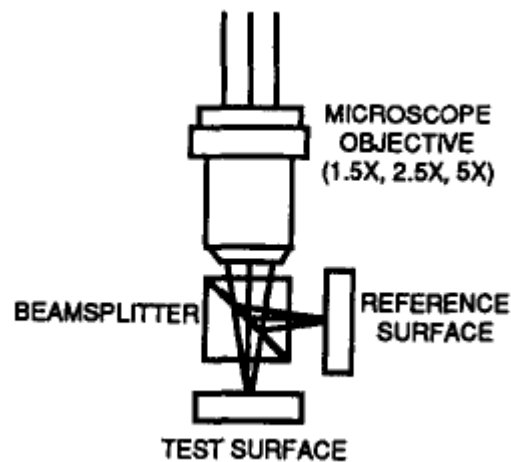


Figure 12a – The Michelson objective [12]

The Mirau interferometer is used for medium magnifications such as 10X, 20X and 40X. It also has the advantage that only a single objective is needed. Even though some optics needs to be placed between the objective and the sample, not much space is used when compared with Michelson. The disadvantage of the Mirau is that a central obstruction is present in the system but this is not a problem for medium magnifications since the size of the obstruction is equal to the field of view of the sample.

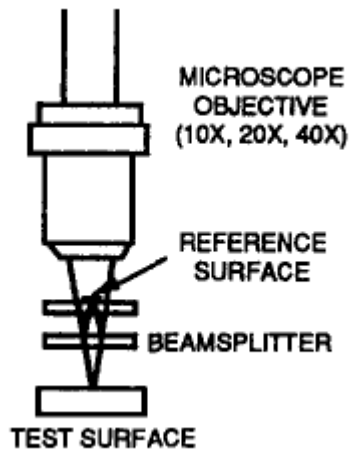


Figure 12b – The Mirau objective [12]

The Linnik interferometer is used for high magnifications such as 100X and 200X. The disadvantage is that two matched objectives are needed. However, since no optics is needed between the objective and the sample, large numerical aperture and short working distance measurement can be performed. Due to large numerical aperture the optical resolution of the system is very high. The optical resolution is given by $0.61\lambda/(2NA)$, where NA is the numerical aperture.

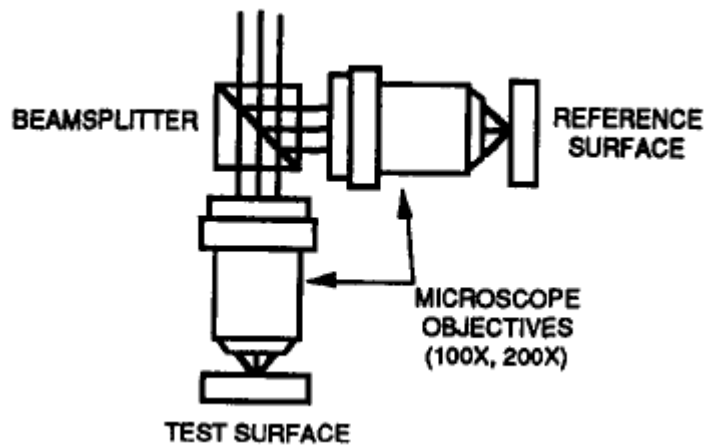


Figure 12c – The Linnik objective[12]

The Mirau interferometric objective is most widely used because only one objective is required for measurement and it offers medium magnification which is right for most applications. Another advantage of this objective is that adjusting the distance for the reference surface is not necessary since it is firmly fixed inside the objective enclosure and hence can be used easily.

A 10X Mirau objective is used in our white light interferometer prototype for medium magnification.

3.3 White-Light Interferometry Equation

In the white-light interferometry, the detected light intensity I is a function of the reference mirror scanning position z and the height of the reflectance layer of the sample z_0 ,

$$I(z) = \int_{\lambda_1}^{\lambda_2} A(z - z_0) B_{Led}(\lambda) B_{Cam}(\lambda) e^{j(k(z-z_0)+\phi)} d\lambda \quad \left(k \equiv \frac{2\pi}{\lambda} \right)$$

where, λ is the wavelength over which the intensity of the light is integrated,

$B_{Led}(\lambda)$ is the complex bandpass of the LED light source,

$B_{Cam}(\lambda)$ is the complex bandpass response of the camera,

and $A(z)$ is the statistical reflection function which depends on the surface roughness.

$$A(z) = C \exp \left[-\frac{z^2}{2\sigma^2} \right]$$

The figure 13 shows the reflection from the surface at precise focus.

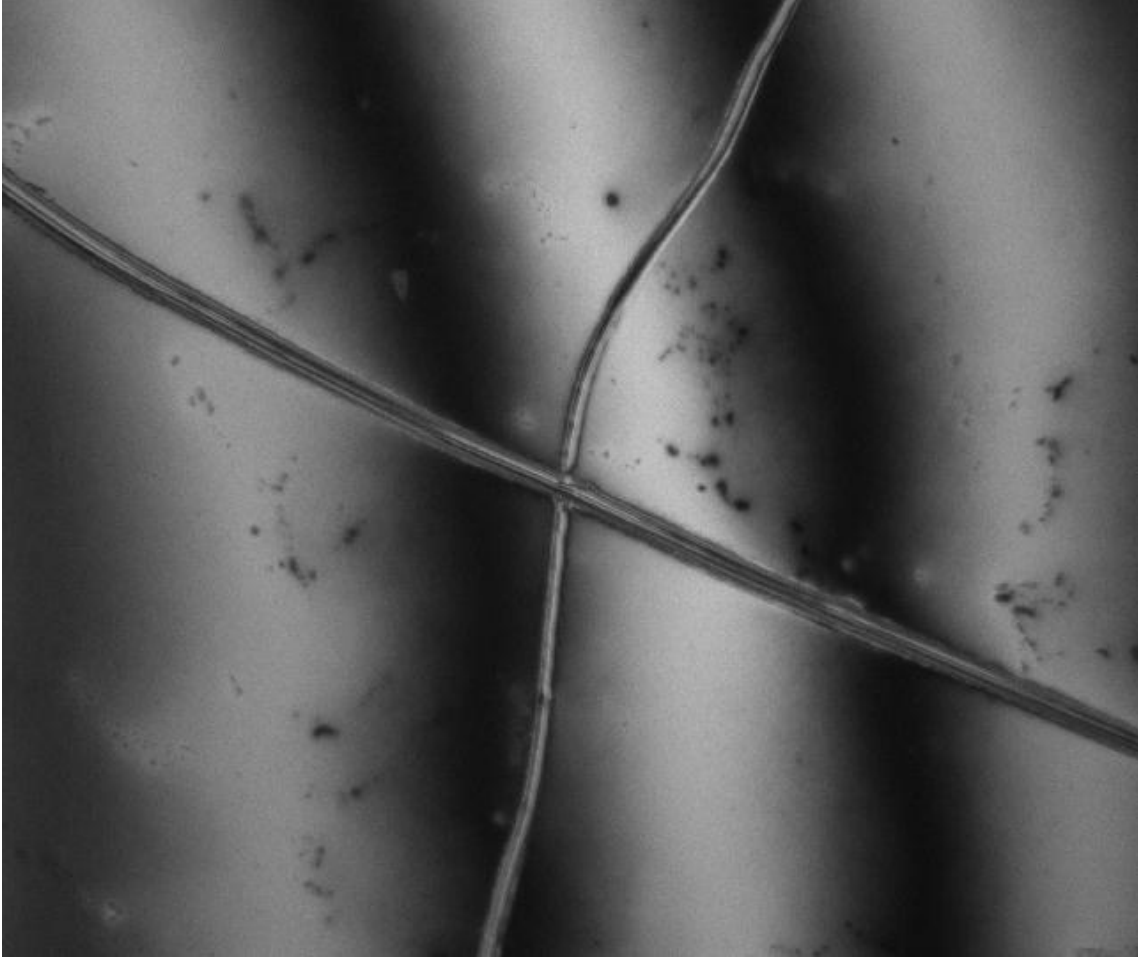


Figure 13 – A raw image of the surface with the intensity envelope

By substituting the above equation, $I(z)$ is expressed in the simple form as a proportional to a sinc function of z .

$$I(z) \propto \frac{\sin z}{z}$$

Where,

$$\phi_0 = -k z_0 + \phi$$

$$a(z) = -\frac{(z - z_0)^2}{2\sigma^2}$$

$$\phi(z) = k z$$

In 3D shape measurements using white-light interferometry, the aim is to obtain the parameter z_0 from the detected light intensity $I(z)$.

3.4 MicroXAM interferometer from ADE Phase Shift

MicroXAM is a white light scanning interferometer which can perform surface topographic measurements using coherence peak scanning and phase measurements techniques. For coherence peak scanning it uses a filtered white light from a halogen lamp. A narrow bandwidth green light is used for phase shift measurements.

First the object to be measured is tested under this interferometer. A software application known as MapView is used to decode the surface topographic information from the interferogram. Then the map files that are obtained from MapView software are given into another program called MountainsMap for the generation of the actual 3d surface visualization.

The scanning process takes a maximum of 30 seconds and the device can scan for a range of 100 μ m using coherence peak scanning.

3.5 Prototype Coherence Peak Scanning Interferometer

3.5.1 Setup

The construction of the device is made as simple as possible while maintaining high quality components for imaging. The basic differences in this new design are that the interferometer is constructed to use only the coherence peak scanning interferometry technique and also that only one piezo motor in the scanning direction is needed. The new design as shown in figure 13 uses a white LED as the light source. The LED and the beam splitter are mounted together on the optical axis. The light from the source is directed towards the surface by the first beam splitter.

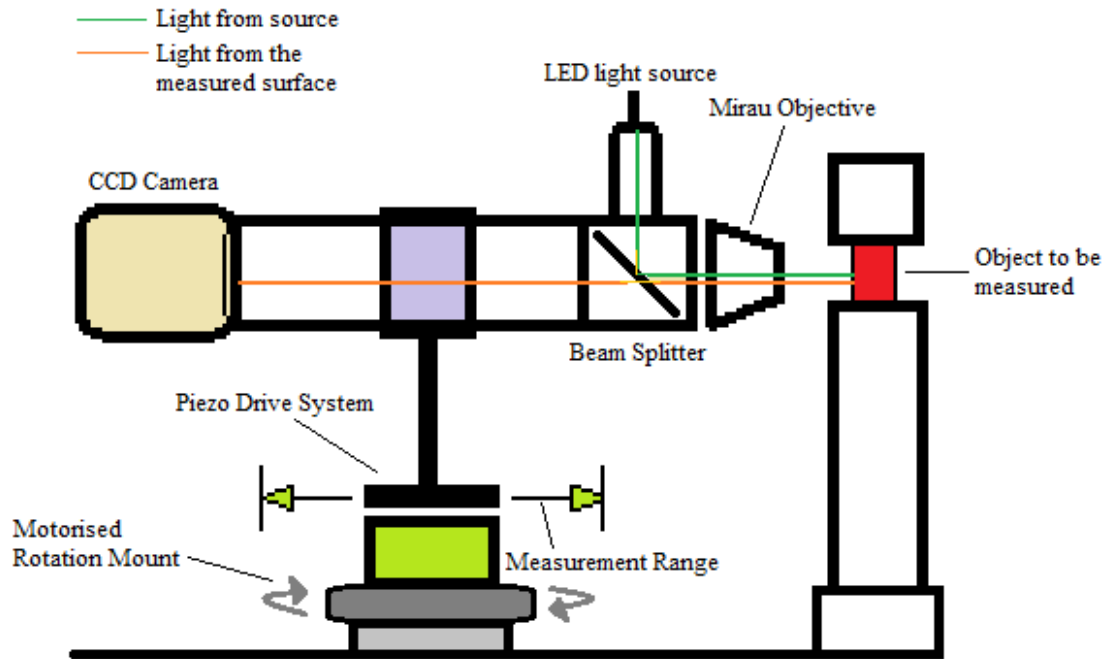


Figure 14 – The prototype interferometer setup

The light is then divided by the beam splitter in the Mirau objective as shown in figure 14. One goes to the reference surface and the other beam is focused on the object under examination.

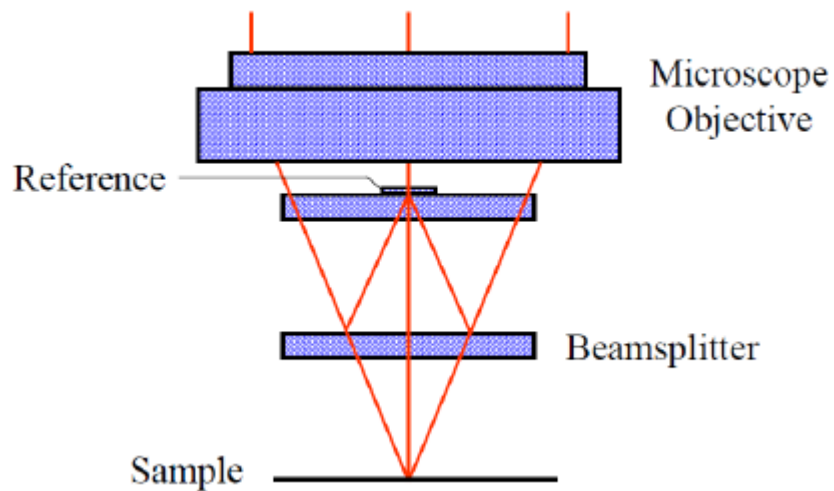


Figure 15 – The sample and the reference mirror setup in a Mirau objective [16]

The resulting pattern is captured by the camera. The piezo motor is used to adjust the focus very precisely in nanometers. The piezo motor is mounted on a motorized rotational stage to align the optical axis perpendicular to the object under measurement.

3.5.2 Interferometer Objective

A 10X Nikon Interferometry objective is used for the setup. The objective has a numerical aperture of 0.3 and a focal length of 20mm. The working distance of the objective is 7.4mm and field of view is 0.88mm x 0.66mm.

3.5.3 Camera

A monochromatic CCD camera Basler piA2400-12gm is used for capturing the images. The maximum resolution of this camera is 2456x2058 and is interfaced by a Gigabit Ethernet port.

3.5.4 Rotor table controller

The rotational table is interfaced to the computer through a compatible controller BSC101 from Thorlabs. The device can be driven through ActiveX controls embedded in the Virtual Interface of LabView. The rotor table is used for aligning the optical axis perpendicular to the object surface.

3.5.5 Piezo drive system

The most important device for the vertical scanning is the Piezo drive system used for precise movements in the order of nanometers. The total range of the system is 20 μ m. The system is used in closed loop for accurate movement. Controller BPC 201 from Thorlabs is used for driving the system and also provides interface for control from LabView.

4 Measurements

4.1 Object under measurement

A polished steel sample with an engraved X mark is taken as the test object since it exhibited both smooth and rough surfaces with height displacements of over 1500nm in the mark. Coherence peak sensing is more advantageous and dominant over phase shift technology when the surface is more rough and the dynamic range exceeds quarter of the wavelength used.

The surface with the X marks is shown in figure 15.

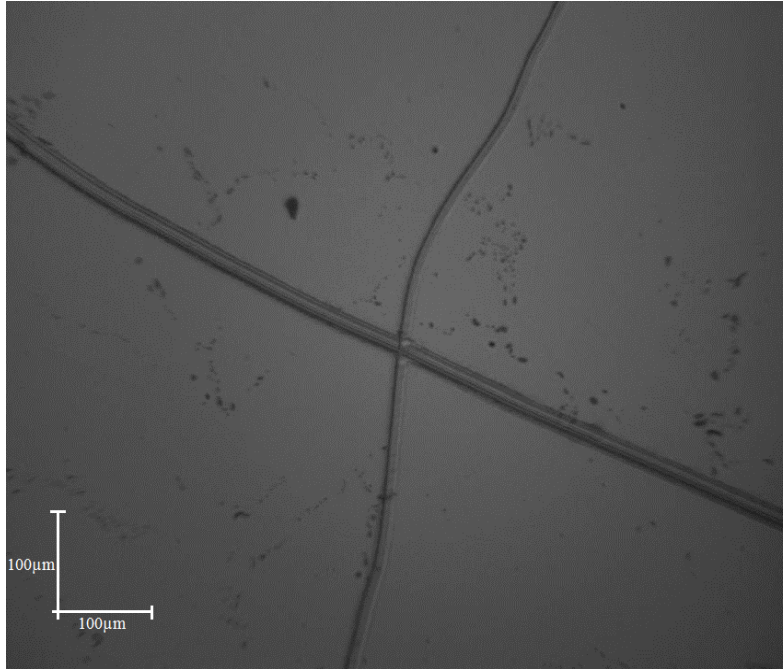


Figure 16 - Sample surface taken as a test object

4.2 Programming the Scanning System

Labview was chosen for developing a GUI for automatic scanning system. ActiveX controls required for interfacing Labview with the controller were available from Thorlabs which makes the use of Labview more convenient. A screenshot of the programmed control interface is shown below.

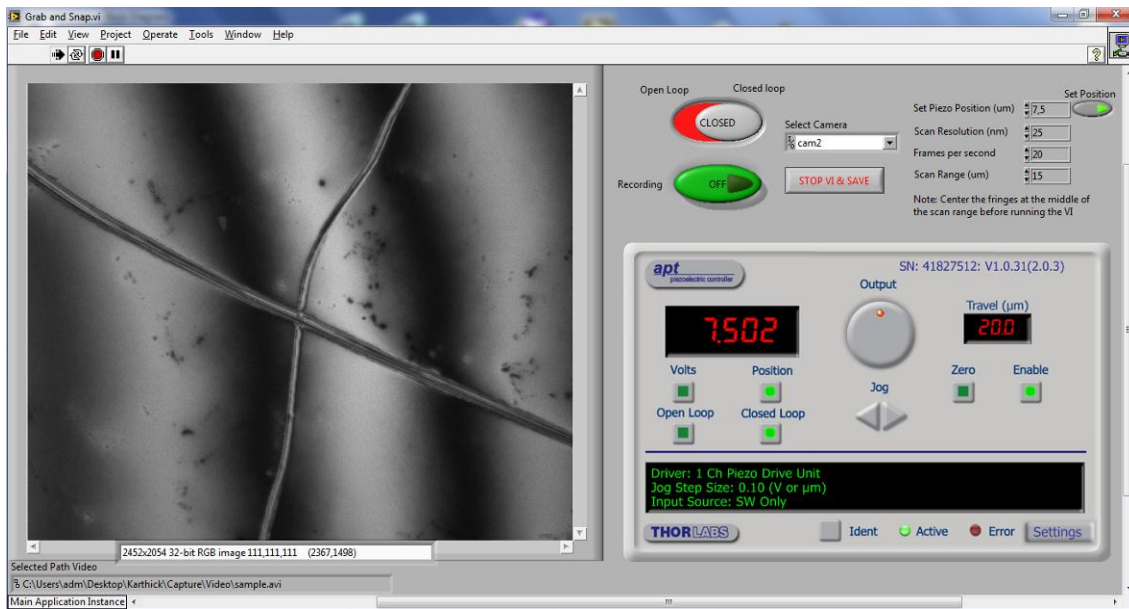


Figure 17a – User interface on LabView for piezo stage control

Parameters required for the scan can be specified before recording the measurements. The system is designed to capture a frame for every step it takes while scanning. The video is saved as an uncompressed AVI file.

The block diagram for the virtual instrument is shown below.

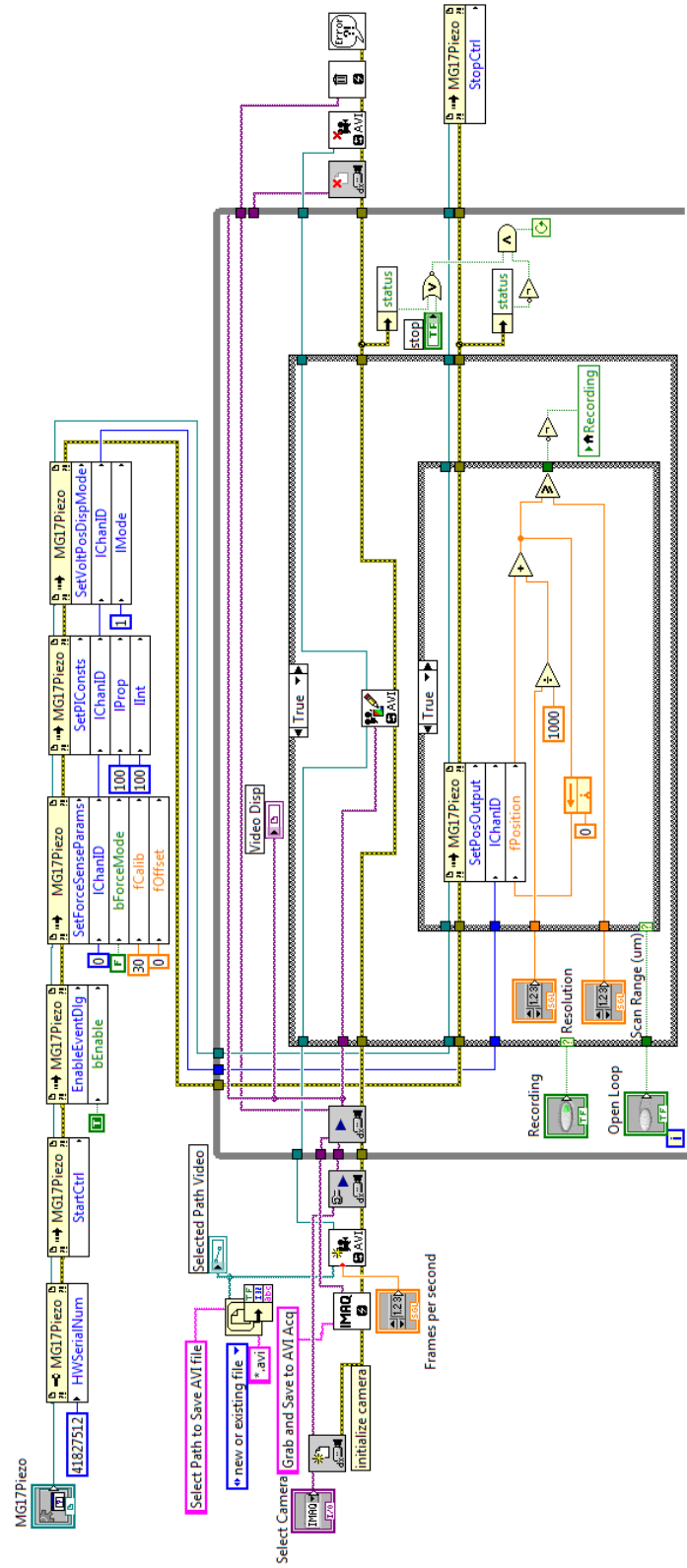


Figure 17b – The control schematic in LabView for piezo stage control

The brightest fringe is positioned at halfway through the scan length before starting the measurements so that the scan is centered to the mean surface level.

4.3 Post processing

The most important part of the whole interferometer system is the processing capability of the system in order to decode the actual surface topography from the captured interferogram. The process of post processing the interferogram should have the ability to reject noise and resolve phase ambiguities. In a coherence peak scanning system the phase ambiguity does not affect the processing since the maximum intensity for a pixel is obtained only when the path lengths are same.

For post processing Matlab from Mathworks is used. The ability to process images as a 2D matrix makes Matlab the right candidate for programming with ease. The program employs the process of splitting the individual frames of the captured video and recognizing the frame at which the intensity was highest for a given pixel. Since there is a direct relation between the frame number and the relative position of the focus while scanning, each pixel is located in 3D space for reconstruction of the surface topography.

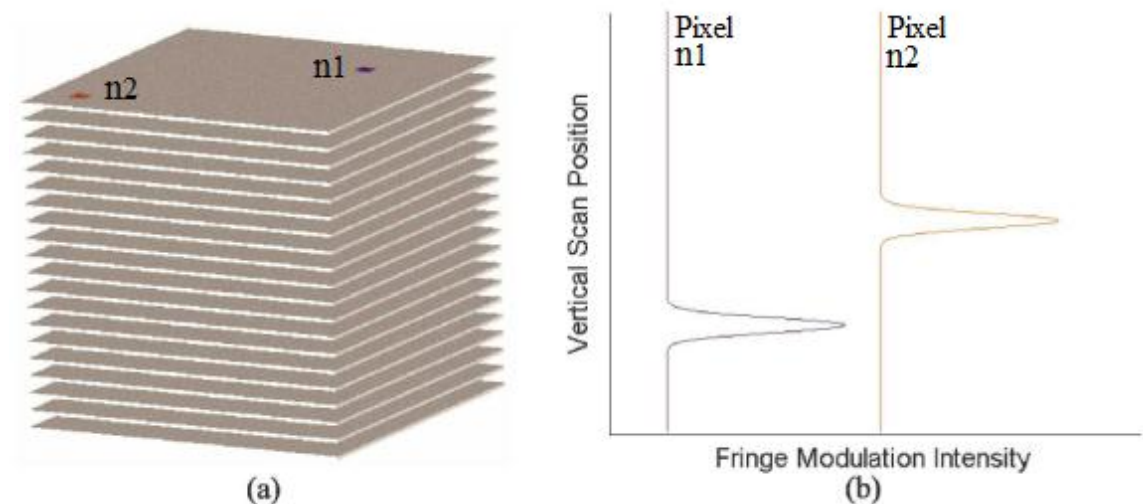


Figure 18 - Construction of 3-D surface through fringe modulation intensity scanning . (a) Each pixel of the sensor is monitored independently as the objective lens is scanned in the vertical direction. (b) After the scan has completed, the fringe modulation intensity profile for each pixel is interrogated for the point of maximum modulated intensity and the corresponding vertical scan position for this condition is established to construct the X-Y-Z coordinate information for the surface as shown for pixels n1 and n2 [18].

The algorithm for post processing of the interferogram in Matlab is shown in figure 18.

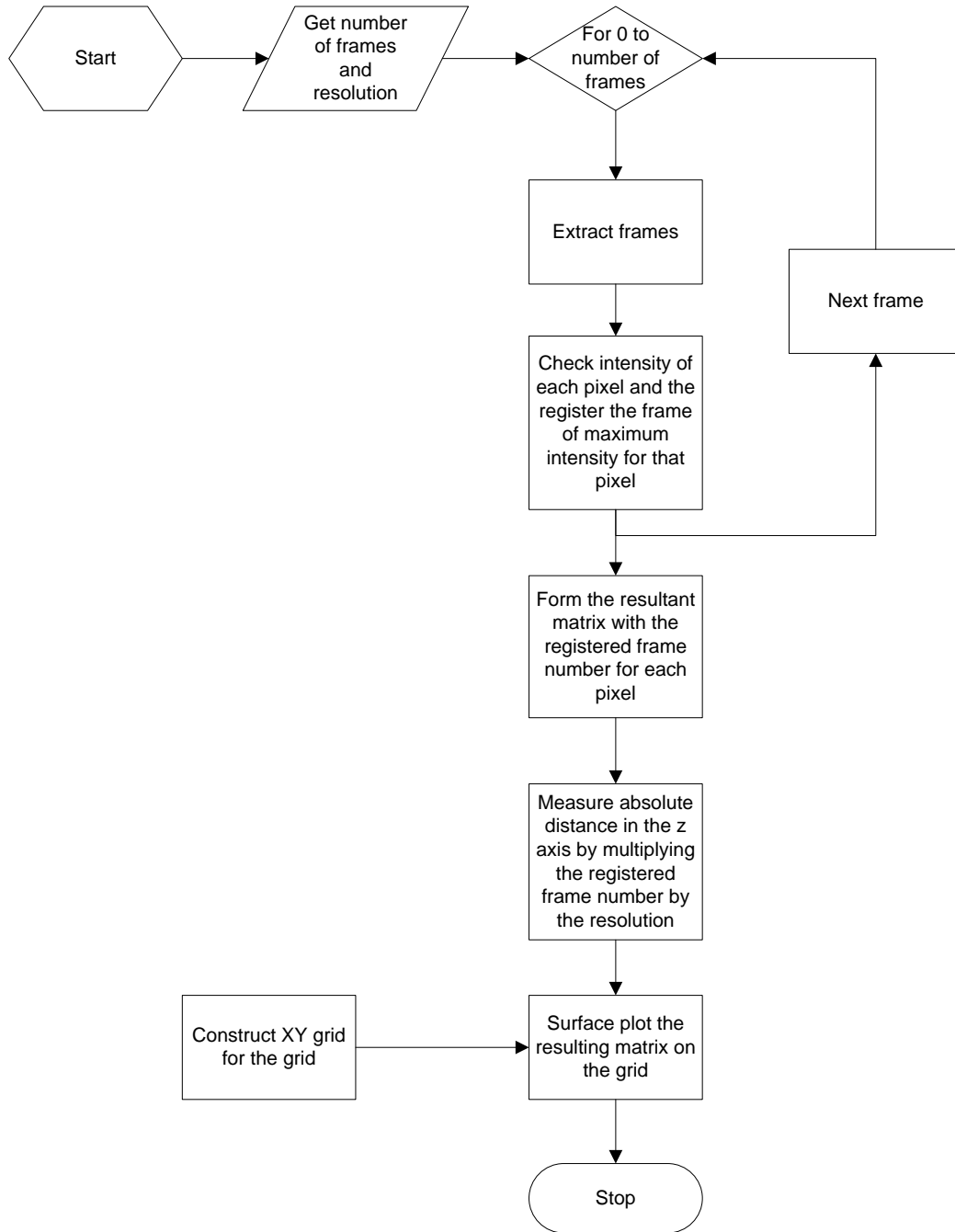


Figure 19 - The processing of interferogram for 3D surface construction

4.4 Results from Prototype Interferometer

The output of the constructed interferometer gave promising data for the examined surface. The data was filtered in order to avoid noise and smoothed to 5 pixels in the xy plane. The visual output of the X mark engraved on the tested polished steel surface looked like the one in figure 19a. The output from the commercial MicroXAM is shown in figure 19b.

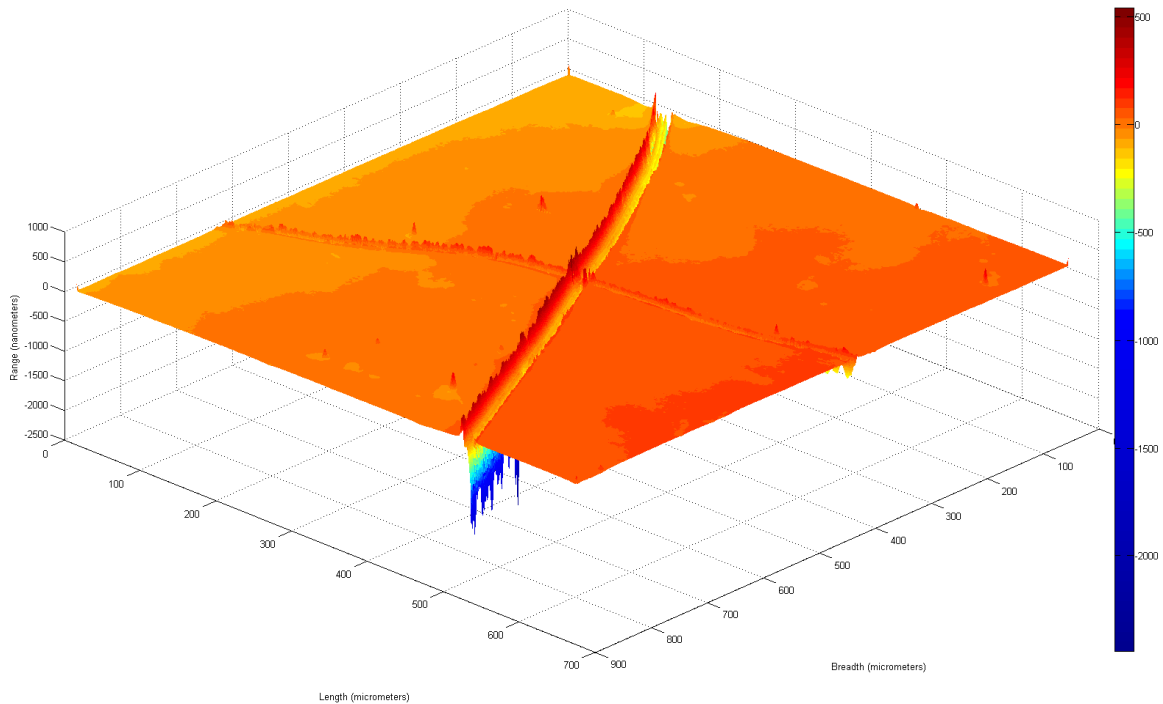


Figure 20a - The constructed 3D surface of the examined object

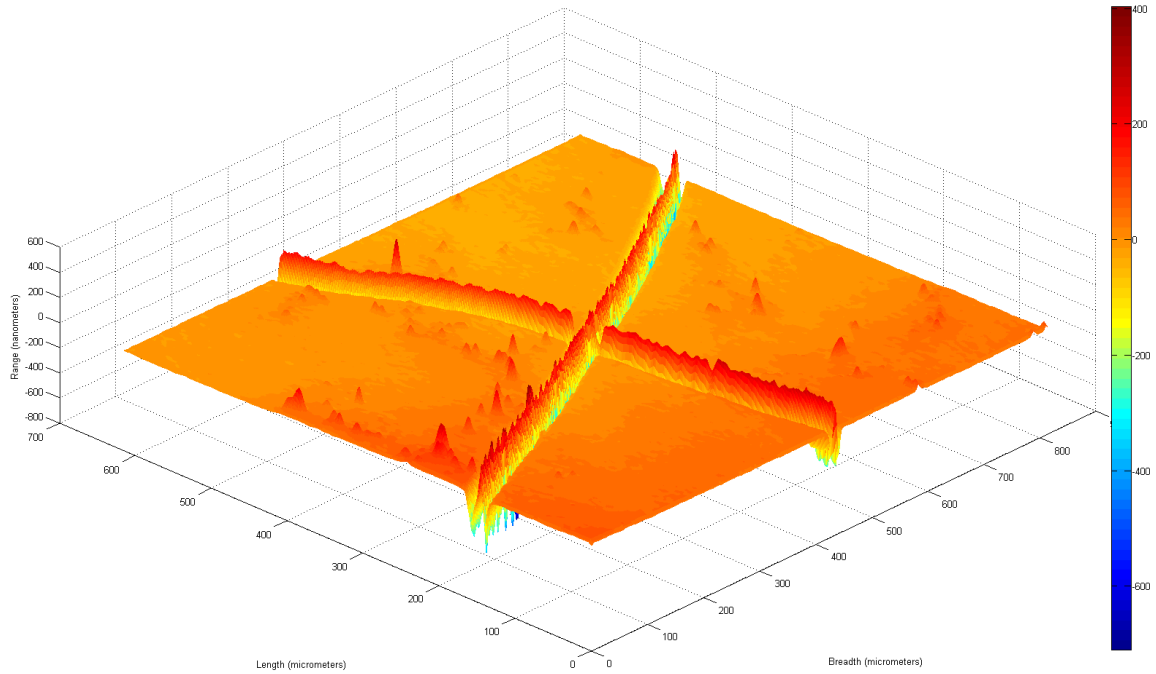


Figure 20b - The constructed 3D surface from MicroXAM data

The peak to valley displacement of the engraved mark was 1500nm on average. The surface was nearly flat around the engraved mark.

4.5 Validation of the prototype interferometer

The result from the prototype constructed is validated by directly comparing it with the results from MicroXAM for the same surface. For this the resulting data from MicroXAM is imported into MATLAB to work with the processed data from the prototype interferometer. The functional flow of the processes is laid out below.

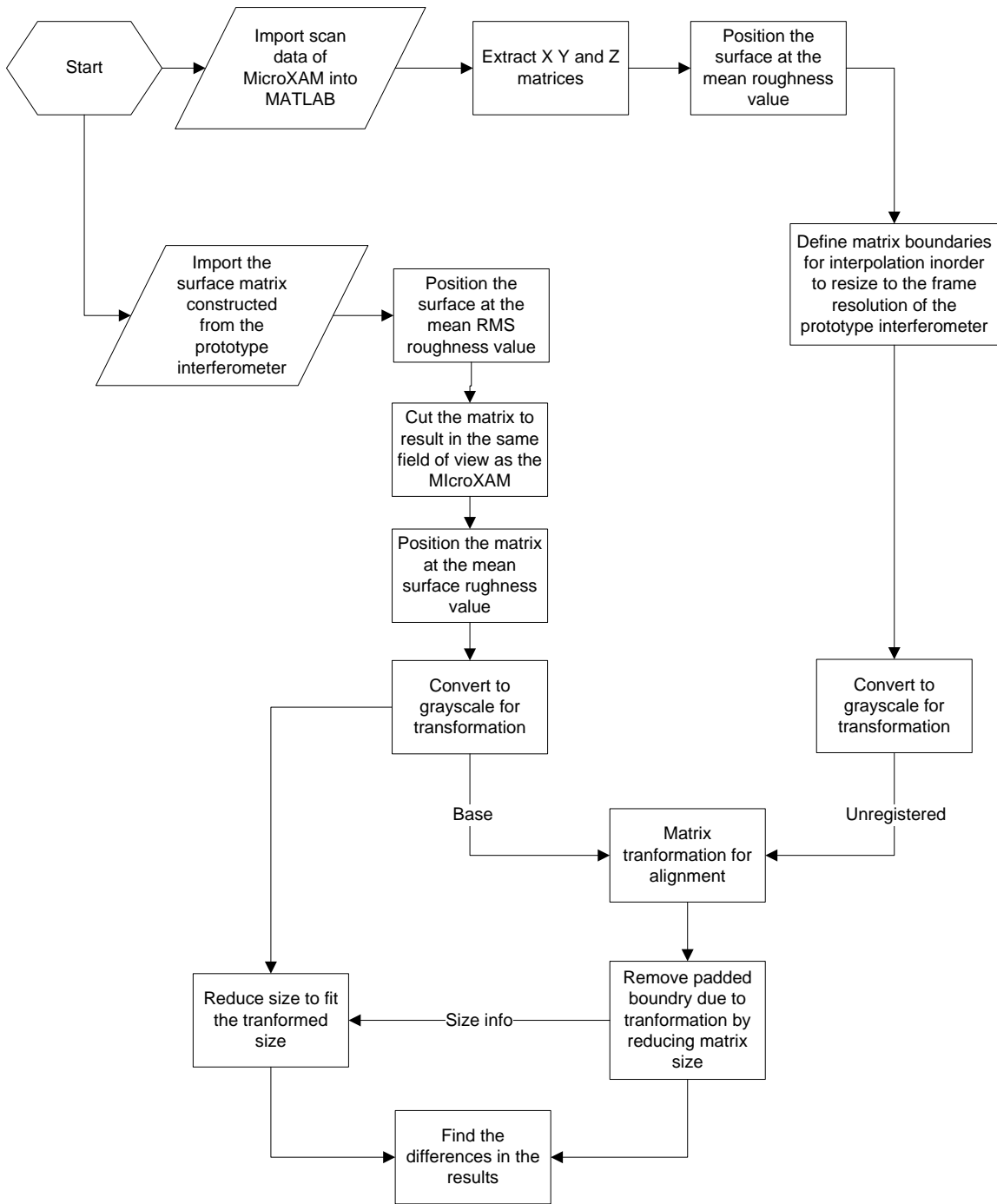


Figure 21 - The process of comparison of results of the two interferograms

4.5.1 Transformation of matrix

The transformation of the matrix actually fits it to a base matrix by rotating and skewing. There were many transformation processes of which ‘nonreflective similarity’ was selected since it gave more accurate transformation of the matrix.

The process of transformation involved pairing of points on the base matrix (from prototype interferometer) and the unregistered matrix (from MicroXAM) by visual examination. A snapshot of the process is shown below.

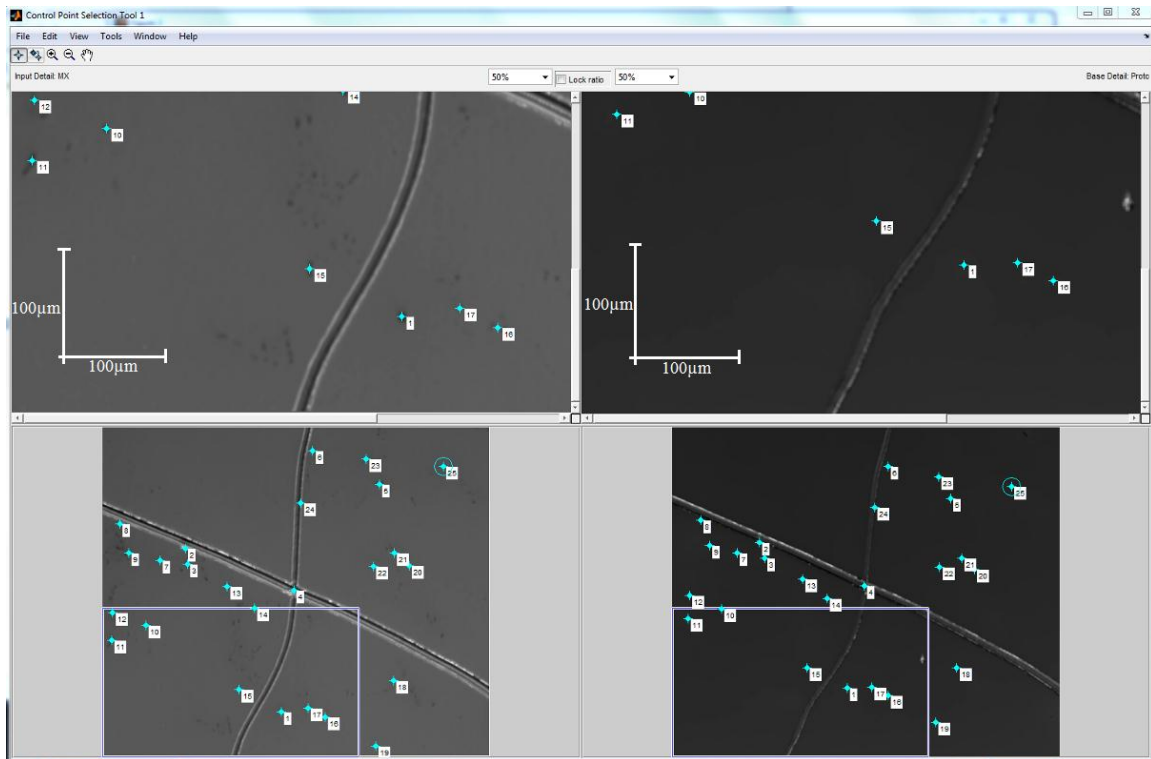


Figure 22 - The process matrix transformation by pairing of points

The image from the prototype interferometer looks dark since the maximum value of the matrix was higher due to dust on the beam splitter and this has brought the surface level to a low scaled value. After pairing the index and base points, the unregistered matrix (from MicroXAM) is changed to fit the matrix data of the constructed interferometer as shown below.

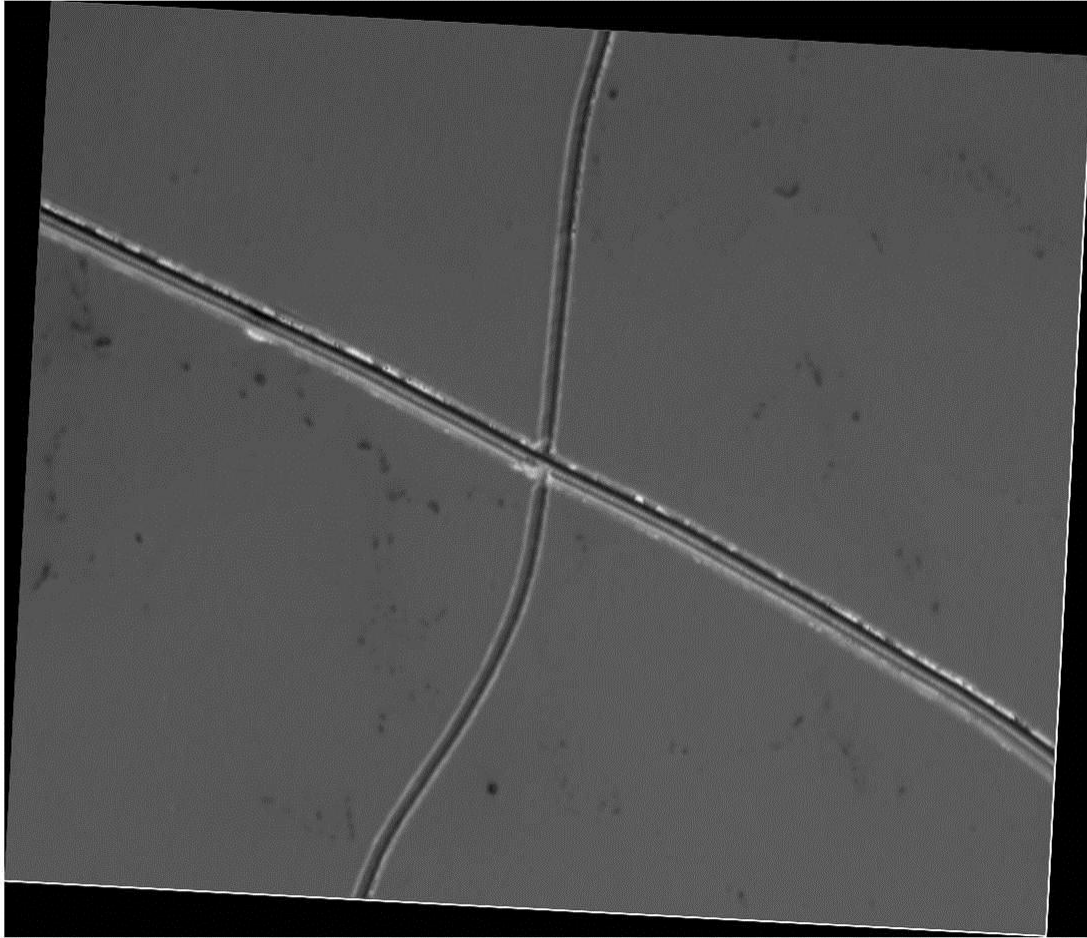


Figure 23 - The transformed image of the matrix

The difference in values between the aligned matrices is analyzed by a difference matrix. The difference matrix gives an average difference of 0.13 in the grayscale on a flat surface which is due to the different scaling of the source matrices. There were some difference in visible spots that can be attributed to less accurate alignment and noise due to dust on the beam splitter used. The difference image of the two matrices in grayscale is shown below.

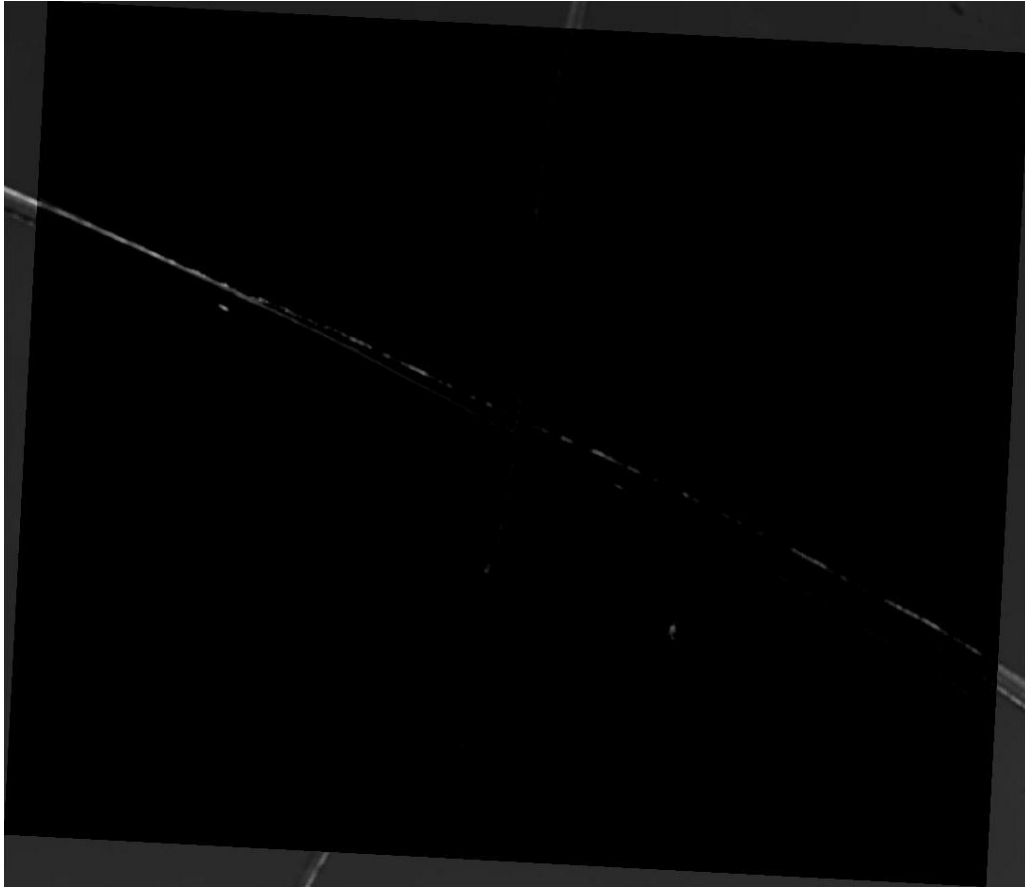
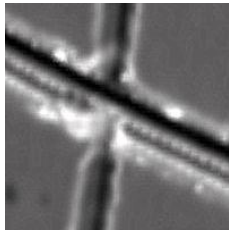
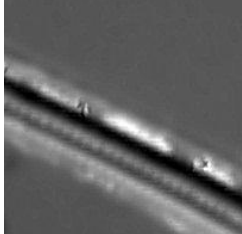

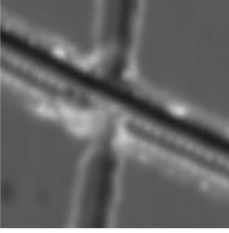
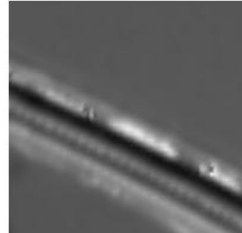



Figure 24 - The difference between the two results as a grayscale image

The standard deviation and mean of the surface topography is analyzed at certain parts of the surface. The sections of 200x200 pixels are used to calculate the difference are shown below.

	Section 1	Section 2	Section 3
Prototype Interferometer			
Commercial MicroXAM			

The calculated standard deviation and mean of the surfaces are given in the table below.

	Standard deviation		Mean	
	Prototype	MicroXAM	Prototype	MicroXAM
Section 1	0.1017	0.1042	0.1624	0.3856
Section 2	0.1078	0.1013	0.169	0.3717
Section 3	0.003	0.0037	0.1342	0.3359

4.5.2 Observations

There is always an uncertainty in the measurement of surfaces with waves and this depends on various parameters of the test setup and of the surface topography of the object measured. Even though the results from the constructed interferometer differs from the commercial interferometer, MicroXAM, we have greatly succeeded in resolving the surface topography of the object upto this level with a minimalistic processing algorithm for analyzing the coherence peak interferogram.

The instrument can be greatly improved by increasing the quality of components such as camera and optics. The processing algorithm even though minimalistic is not quick enough for frequent processing since it is not optimized for speed. It was coded to satisfy the demonstration of the algorithm and its functionality.

There were ambiguities in positioning of the piezo stage even in closed loop because its offset adds to the total distance after a set of steps.

The noise due to the camera was significant and was removed with the reduction of resolution due to filtering. A high quality camera with a cooled CCD or a CCD with less heat dissipation can provide more accurate data of the surface due to less noise figure.

The optics should be cleansed on a regular basis to avoid enlarged noise due to unwanted dust particles over the light path. An example of noise due to dust is shown in figure 24.

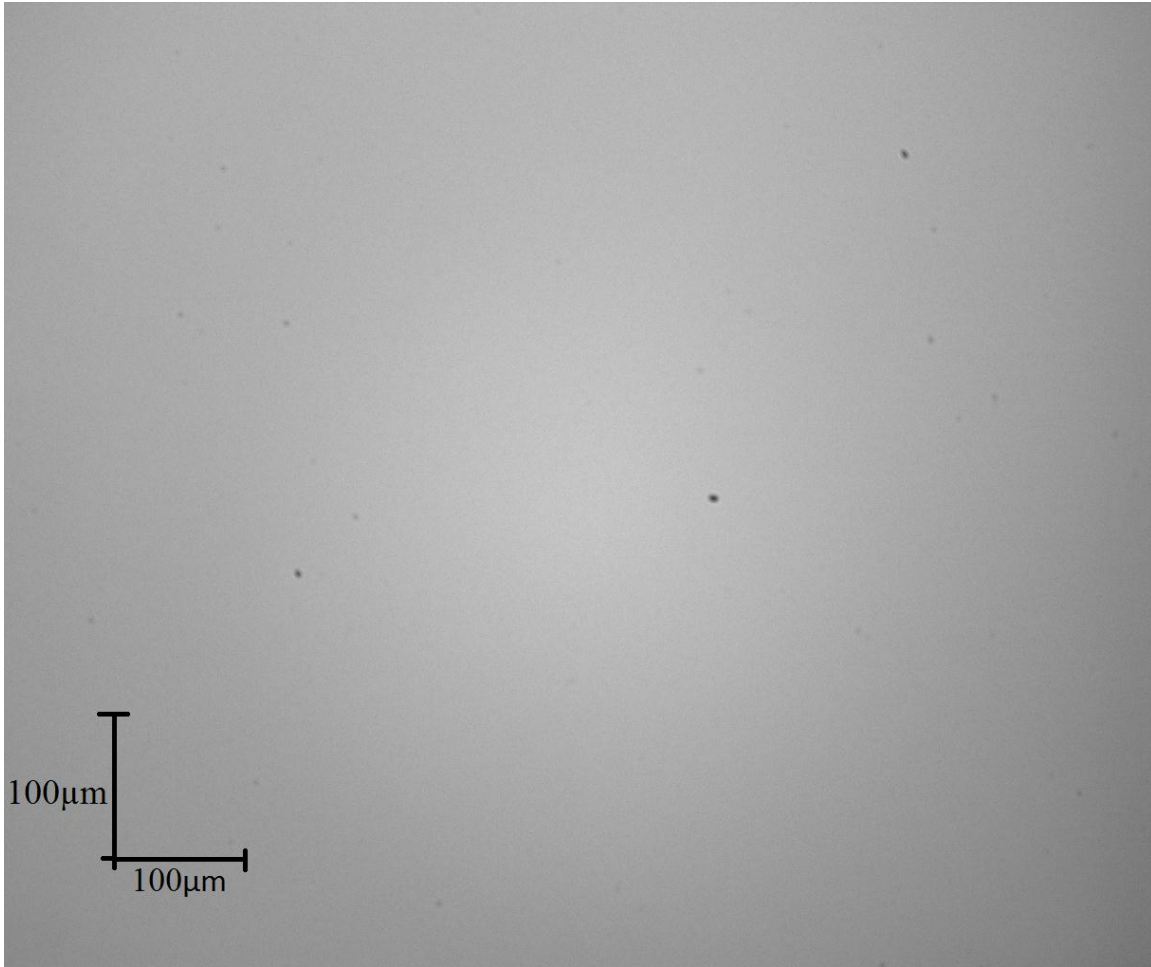


Figure 25 - The dust spots on the beam splitter

5 Possible Design

The interferometer was constructed with a rotational stage for adjustment of the optical axis perpendicular to the surface. In case of a cylindrical surface, example a part of a bore of an engine, the analysis can be done as sections and stitched together later to form a rectangular surface as a result which can be visualized radially using advanced 3D soft wares.

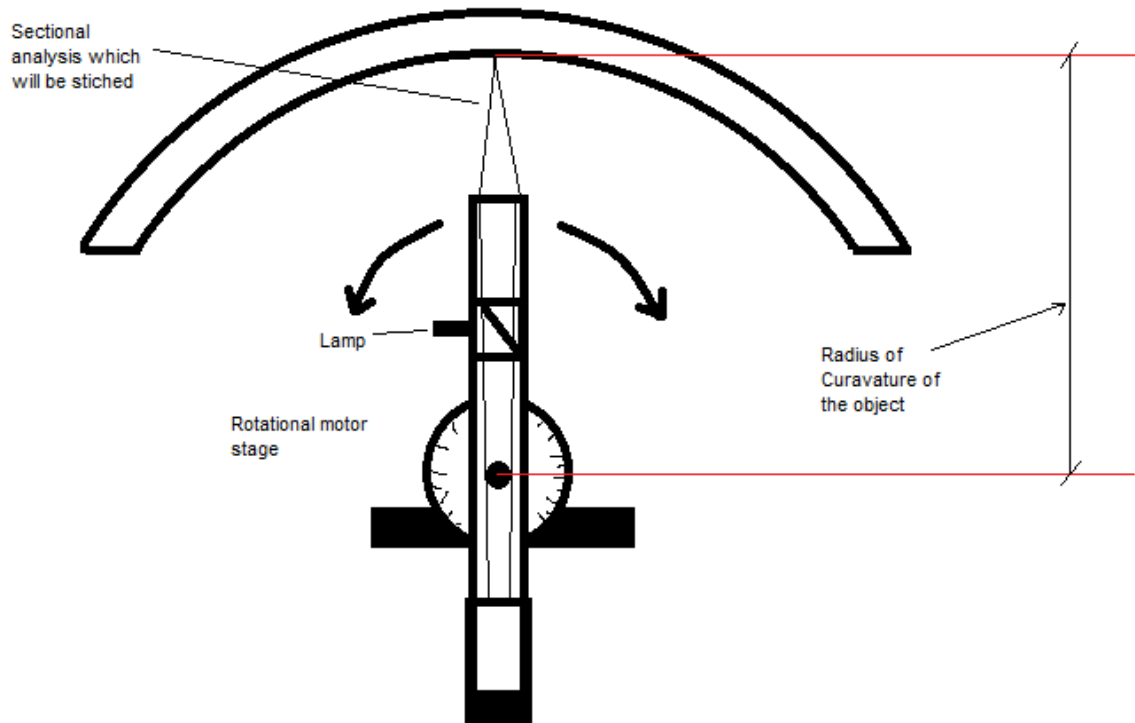


Figure 26 - The possible design of the interferometer to scan a cylindrical surface

Here the placement of the camera on the stage with the nano-track so that all are aligned at the center of curvature of the object is a great concern. Achieving this, a great success to this experiment is evident. Here the rotational step of the stage and the hysteresis of the motor is another major problem to be solved.

6 Conclusions

A coherence peak interferometric surface topographer has been designed and implemented for surface profiling. We have proved that a interferometer can be simple in construction and portable. The setup and processing of the interferogram is also included in this project.

Our practical experiment in constructing the interferometer has proved that the system is simple to design and that it can map the topography of a surface with the same resolution as that of commercially available interferometers. The observed validation process proved slight deviations in the results from the prototype interferometer but the overall surface mapping was satisfactory and can be improved by suggested points from the observations. Once the initial setup is complete, the measurement of a surface and its processing are simple even though the processing is not optimized for time.

Additional designs provided on this topic can be constructed for profiling different surfaces with even improved accuracy.

7 References

- [1] Pal, Bishnu P, *Fundamentals of Fibre Optics in Telecommunication and Sensor Systems*. New Delhi: New Age International. p. 663 (read section 3). ISBN 8122404693, 1992.
- [2] Eugene Hecht, *Optics, Fourth edition*, ISBN 0-321-18878-0.
- [3] M. Davidson, K. Kaufman, I. Mazor, and F. Cohen, *An Application of Interference Microscopy to Integrated Circuit Inspection and Metrology*, Proc. SPIE, 775, 233-247, 1987.
- [4] G. S. Kino and S. Chim, *Mirau Correlation Microscope*, Appl. Opt. 29, pp. 3775-3783, 1990.
- [5] T. Dresel, G. Hausler, and H. Venzke, *Three-dimensional sensing of rough surfaces by coherence radar*, Appl. Opt. 31(7):919-3925, 1992.
- [6] P. J. Caber, *An Interferometric Profiler for Rough Surfaces*, Appl. Opt. 32 (19), pp. 3438-3441, 1993.
- [7] James C. Wyant, *Computerized interferometric measurement of surface microstructure*, Proc. SPIE 2576, pp.122-130, 1995.
- [8] J. C. Wyant, *Laser Focus World (September)*, 131-135, 1993.
- [9] N. Balasubramanian, U.S. Patent #4,340,306, Jul. 20, 1982.
- [10] P. J. Caber, Appl. Opt. 32(19), 3438-3441, 1993.
- [11] Gordon S. Kino and Stanley S.C. Chim, Appl. Opt. 29(26), 3775-3783, 1990.
- [12] James C. Wyant and Katherine Creath, *Advances in Interferometric Optical Profiling*, Int. J. Mach. Tools Manufact. Vol. 32, No. 1/2, pp. 5-10, 1992.
- [13] Cohen, D.K., E.R. Cochran, and J.D. Ayres, *Development of an automatic focusing mechanism for an interference microscope*. Proc. SPIE, 1164, 1989.
- [14] Creath. K, *Step height measurement using two-wavelength phase-shifting interferometry*, Appl. Opt. 26, 2810-2816, 1987.
- [15] <http://www.rp-photonics.com/coherence.html>

[16] Wikimedia Commons

[17] James C. Wyant , *White Light Interferometry*, Optical Sciences Center.

[18] Santo Padula II, *Measurement Variability of Vertical Scanning Interferometry Tool Used for Orbiter Window Defect Assessment*, NASA/TM—2009-215636.